

**Assembly Synthesis of Cu₂O-on-Cu Nanowires with Visible-light Enhanced Photocatalytic Activity**

Journal:	<i>Dalton Transactions</i>
Manuscript ID:	DT-ART-04-2015-001393.R1
Article Type:	Paper
Date Submitted by the Author:	12-Jul-2015
Complete List of Authors:	Chen, Hanxing; Tongji University, Chemistry Tu, Teng; Tongji University, Chemistry Wen, Ming; Tongji University, Department of Chemistry Wu, Qingsheng; Tongji University, Chemistry



Journal Name

ARTICLE

Assembly Synthesis of Cu₂O-on-Cu Nanowires with Visible-light Enhanced Photocatalytic Activity

Hanxing Chen,[†] Teng Tu,[†] Ming Wen,^{*} and Qingsheng Wu,^{*}

Received 00th January 20xx,
Accepted 00th January 20xx

DOI: 10.1039/x0xx00000x

www.rsc.org/

New Cu₂O-on-Cu nanowires (NWs) are constructed for developing the visible-light-driving activity of photo-catalysts via a facile self-assembly followed in-situ reduction approach of Cu₂O nanoparticles (NPs) on Cu NWs surface assisted by structure-director. In the resultant Cu₂O-on-Cu NWs, the Cu₂O NPs with the diameter of 10 nm show well distribution on the 50 nm sized Cu single-crystal NWs. Owing to the band-gap adjusting effect and high electron transportation, the coupling of narrow-band-gap semiconductor Cu₂O and excellent conductor Cu can lead to the markedly enhanced high visible-light photocatalytic activity of Cu₂O-on-Cu NWs toward the degradation of dye pollutant including Rhodamine B (RhB), methyl orange (MO) and methyl blue (MB), respectively. As-designed Cu₂O-on-Cu heterostructured NWs exhibit higher-performance for the catalytic degradation of die compounds compare with pure Cu₂O. Nearly 60%, 100%, and 85% conversion with the reaction rate constant (k) of 0.0137, 0.0746 and 0.0599 min⁻¹ can be achieved for the degradation of RhB, MO and MB, respectively. Besides the high efficient transportation of electron, Cu NWs have strong capacity for oxygen activation which results in the gathering of negative charges and rich chemisorbed oxygen onto the surface, it can be responsible for high catalytic efficiency of Cu₂O-on-Cu NWs toward the degradation of organic pollutant.

Keywords: Cu₂O-on-Cu nanowires, Visible-light-driving photocatalysis, Narrow-band-gap semiconductor of Cu₂O, Dye pollutant

Introduction

One-dimensional (1D) metal-semiconductor heterostructured nanowires (NWs) have been proven to have promising potential in diverse fields such as catalysis, electronics, energy storage and solar utilization due to their unique advanced optical, electrical and catalytic properties, especially in the catalytic industry.¹⁻⁸ A variety of investigation for metal-semiconductor composite nanostructures has been funded that the incorporation of 1D metal building blocks and semiconductor into integrated heterostructured photo-catalysts benefits to get highly efficient separation and transfer of photoinduced charges.^{4,5,8} But on the other side, it is still challengeable to fabricate the visible-light induced 1D photocatalysts.^{1,2,9-15}

The semiconductor photocatalytic technique exhibits a great potential toward finding a remedy for continuous

anthropogenic deterioration of environment. The common photocatalysts for environmental remediation are primarily metal oxides with different band gaps. The working range of the wide band gap semiconductors are limited only to the UV light irradiation which is hardly 5% of the entire spectrum of the incident solar light on the earth.¹⁶⁻²⁰ Therefore, it is essential to develop a fresh material with a narrow band gap which can directly be applied for the utilization of the visible range light irradiations. The development of perspective visible-light photocatalysts has gained a significant interest in recent years because of their energy- and environment-related applications, such as clean energy production, photoelectrochemical process, and environmental needs under solar light. However, the fabrication of 1D well visible-light-driven efficiency photocatalysts still shortage well proposed yet. Meanwhile, few research works have been reported about the economical metal-semiconductor visible-light-driven photocatalysts with high activity and high electron transportation rate.^{11-13,21-29} But it is still a big challenge to develop the visible-light-driven catalysis.

Cuprous oxide (Cu₂O) is a p-type narrow-band-gap semiconductor with a direct bandgap of 2.17 eV and it is widely studied in the fields of solar energy conversion and micro/nanoelectronics.^{30,31} Lots of effort have been performed for the fabrication of Cu₂O nanocomposites, such as

Department of Chemistry, Key Laboratory of Yangtze River Water Environment, Ministry of Education, Tongji University, 1239 Siping Road, Shanghai 200092, China.

E-mail: m_wen@tongji.edu.cn (Ming WEN); qswu@tongji.edu.cn (Qingsheng WU)
Fax: (+) 86-21-65981097

[†] These authors contributed equally to this work.

Electronic Supplementary Information (ESI) available: Further details SEM images and UV-vis spectra. See DOI: 10.1039/b000000x/.

Cu₂O@TiO₂ core-shell exhibiting higher photocatalytic activity than that of the single phase catalyst in the degradation of 4-nitrophenol;³² Ultra-small Cu₂O nanoparticles (NPs) loaded Cu₂O nanosheet present the enhanced visible-light activity induced by Cu₂O-Ti₂O via the increase of the electron-hole separation;³³ TiO₂/Cu₂O composites can degrade Reactive Red X-3B under visible light while the pure phase Cu₂O show negligible activity³⁴ and so on. However, low quantum efficiency and photocorrosion of Cu₂O hamper its photocatalytic applications. Functional groups that trap photo-excited electrons can absorb metal ions with positive charge and form compound particles on the sheet surface under light irradiation. Cu metals with high carrier transport rates can serve as transport channels between semiconductor materials.³⁵ The coupling of Cu and Cu₂O into a proper hetero-architecture can effectively facilitate the separation of photogenerated electrons and holes between Cu and Cu₂O, and their performance can be greatly enhanced.³⁶ Furthermore, doping Cu₂O with transition metal Cu for narrowing band gap can enhance the absorption of visible light. The strategy of metal-core 1D hybrid composites was proposed to improve the performance of Cu₂O by suppressing the charge recombination and increasing the formation of active species by trapping photogenerated electrons. Copper-based nanomaterials are of particular interest because of their high electrical conductivity.

In this work, Cu₂O-on-Cu heterostructured nanowires (NWs) have been constructed through facile self-assembly followed in-situ reduction synthesis under magnetic stirring, in which the Cu₂O NPs show well distribution on Cu NWs. The photocatalysis activity has been investigated in detail for the potential applications. The resultant Cu₂O-on-Cu NWs exhibit excellent performance to the catalytic degradation of Rhodamine B (RhB), methyl orange (MO) and methyl blue (MB) under visible-light irradiation, due to the hierarchical nanostructures and the synergistic effect between metal Cu NWs and Cu₂O NPs.

Experimental Section

Chemicals

Glucose (C₆H₁₂O₆, 99.5%), 1-Hexadecylamine (HDA, 90.0%), Copper (II) chloride dihydrate (CuCl₂•2H₂O, 99.0%), Copper (II) acetate (C₄H₈CuO₅, 98%) were purchased from Aladdin Chemical Reagent Co. Ltd. Ethyl Alcohol (C₂H₆O, 99.5%), Sodium Hydroxide (NaOH, 90%) were purchased from Sinopharm Chemical Reagent Co., Ltd. All the reagents were analytical purity and used without further purification.

Preparation of Cu NWs

21 mg CuCl₂•2H₂O, 50 mg glucose, 180 mg HDA and 10 mL deionized water were added into a small glass bottle with cap. The final solution was stirred overnight with a magnetic stir plate at room temperature. Then, this system was transferred into a oil bath and heated to 110°C and held with magnetic stirring for 6 h. The color of the final solution was reddish-

brown. The Cu NWs were rinsed by deionized water and ethyl alcohol alternately, which was propitious to the following experiment.

Synthesis of Cu₂O-on-Cu NWs

100mg copper acetate and 100 mL deionized water were mixed in an erlenmeyer flask (5 mM). The prepared Cu NWs was added into this homogeneous solution. The new system was firstly stirred magnetically for 0.5 h, then was put into oil bath at a temperature of 50°C. After adding 8 mL 40 mg/L NaOH, the system was stirred for 2 min, followed by adding 8ml 0.05g/L glucose, then the system was kept in oil bath for 1 h. After the system was cooled to room temperature, the resulting product was removed from the solution, rinsed thoroughly with deionized water and ethyl alcohol for three times. The product was stored in ethyl alcohol finally.

Characterization

The size and morphology of the Cu@Cu₂O nanostructure were examined by a HITACHIS-4800 (Japan) Field-emission scanning electron microscopy (FE-SEM), a JEM-2100 (Japan) transmission electron microscopy (TEM), high-resolution transmission electron microscopy (HRTEM) and selected-area electron diffraction pattern (SAED), respectively. Element analysis was measured by energy dispersive X-ray spectroscopy (EDS) conducted at 20 keV on an EMAX X-act EDS instrument (Horiba). The powder X-ray diffraction analysis (XRD) patterns were characterized by Bruker D8 (German) diffractometer with a Cu K α X-ray radiation source (λ = 0.154056 nm). X-ray Photoelectron Spectroscopy (XPS) experiments were carried out on an Axis Ultra DLD system (Shimadzu) using Al K radiation ($h\nu$ =1486.6 eV). The whole spectra (0~1200eV) and the narrow spectra of all the elements with much high resolution were both recorded by using RBD 147 interface (RBD Enterprises, USA) through the AugerScan 3.21 software. Binding energies were calibrated by using the containment carbon (C1s=284.6eV). The specific surface areas of the samples were determined through nitrogen adsorption at 77 K on the basis of Brunner-Emmet-Teller (BET) equation using a Micromeritics ASAP 2020 V3.00 H.

Photocatalytic degradation test

We have compared the photooxidation ability of the as-prepared materials Cu NWs, Cu₂O and Cu₂O-on-Cu heterostructured NWs. The photocatalytic activities of the prepared catalysts were evaluated by the degradation of carcinogenic and mutagenic organic dye pollutant, including RhB, MO, and MB. The photocatalytic tests were carried on in a reaction chamber equipped with a cooling water-cycle system to keep a stable temperature. A 500W tungsten lamp was used as the light source. In a typical visible-light photocatalytic experiment, 10 mg of the catalyst was dispersed in 50 mL RhB, MO, and MB (50 μ g•L⁻¹) aqueous solution separately, and the obtained suspension was magnetically stirred in the dark for 1 h to achieve adsorption-desorption equilibrium. During beam, 3 mL of the suspension was withdrawn periodically from the reactor chamber,

followed by centrifugation and filtration, and the obtained clear solution was analyzed by ultraviolet visible spectrophotometer (8453 UV/VIS, Agilent). The degradation rate of organic pollutant was calculated by the following equation: $C/C_0=A/A_0$ and $\ln(C/C_0)=\ln(A/A_0)$, where C_0 and A_0 separately stands for the initial concentration of organic pollutant solution and initial absorbance of solution; C and A separately stands for the concentration of organic pollutant solution after the irradiation of tungsten lamp and the absorbance of solution at any time.

Results and Discussion

Structures and Characterization

FE-SEM and TEM were employed to monitor initially morphology of as-obtained Cu_2O -on-Cu NWs, as shown in Figure 1. The diameters of Cu NWs before and after coated Cu_2O were ~ 50 nm and ~ 90 nm, respectively. As observed in Figure 1D and E, Cu_2O NPs with the mean diameter of ~ 10 nm arrange along the surface of Cu NWs uniformly. After loading with Cu_2O NPs, the Cu NWs well maintain the original NW shape. Figure 1C shows the SAED recorded from single Cu NW gives the single crystal diffraction pattern with the indexed plane of (110) and (200). The HRTEM image of the interface between Cu_2O and Cu is characterized and presented in Figure 1 F with the inset SAED pattern. It can be clearly observed the lattice fringes with space of 0.302 nm for Cu_2O (110) planes and 0.209 nm for Cu (111) planes. Its corresponding SAED gives rise to the combination diffraction pattern of Cu_2O single-crystal together with Cu crystalline spot of Cu [111] and Cu_2O [110] zones diffractions. All these observations indicate the present self-assembly method is highly effective to obtain uniformly loaded Cu_2O NPs on Cu NWs. In the fabrication process, the reaction conditions including the different concentration of Cu_2O precursor solution, and heating temperatures all have been respectively investigated, and shown in Figure S1, S2 in Electronic Supplementary Information (ESI). In addition, the specific

surface area of bare Cu_2O and Cu_2O -on-Cu NWs were determined using nitrogen-gas adsorption method. It is a very important factor influence the catalytic activity. The BET surface of Cu_2O -on-Cu NWs ($75.2 \text{ m}^2\text{g}^{-1}$) is higher than bare Cu_2O NPs ($58.3 \text{ m}^2\text{g}^{-1}$), which endows the materials with the increasing photoabsorption sites and results in the promotion of activity.

Figure 2 exhibits the morphologies of Cu NWs, Cu_2O NPs and Cu_2O -on-Cu composite NWs together with their corresponding EDS analysis and XRD patterns. As for the results of Cu_2O -on-Cu NWs, it compromises the information of Cu_2O and Cu, respectively. In Figure 2B, the EDS analysis of Cu NWs (Ba) shows dominant Cu element, and that of Cu_2O NPs (Bb) illustrates more Cu peaks with higher atomic ratio of O elements and reveals that the Cu:O atomic ratio to

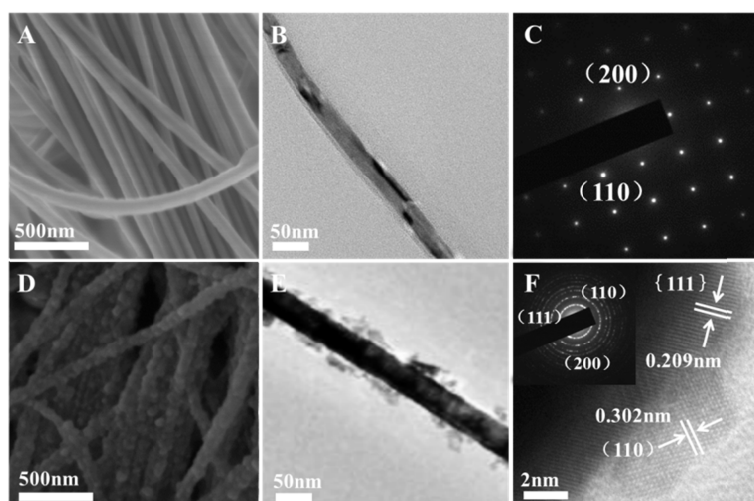


Figure 1. SEM (A) and TEM (B) images together with SAED pattern (C) of Cu NWs; SEM (D) and TEM (E) images as well as HRTEM image with inset SAED pattern (F) of Cu_2O -on-Cu NWs.

be 2:1, so Cu_2O is the stoichiometric compound. As for (Bc), the atomic ratio of Cu:O=3:1 for Cu_2O -on-Cu NWs agrees well with the raw material ratio. The XRD patterns in Figure 2C correspond to Cu NWs (Ca), Cu_2O NPs (Cb) and Cu_2O -on-Cu NWs (Cc), respectively. Cu XRD pattern shows three broad halos of (111) at 43.3° , (200) at 50.5° , (220) at 74.1° , respectively, which agrees well with the face centered cubic (fcc) lattice of Cu NWs (JCPDF#65-9026). All diffraction peaks of Cu_2O NPs belong to cubic Cu_2O phase (space group: Pn-3m ; $a_0 = 4.27 \text{ \AA}$; JCPDS#05-0667). The XRD pattern of as-prepared Cu_2O -on-Cu NWs is shown in Figure 2 Cc and it matches to the mechanical superposition of Cu patterns and Cu_2O patterns, confirming the fabrication hierarchical heterostructured Cu_2O -on-Cu NWs.

In order to confirm the formation and bonding information of Cu_2O -on-Cu NWs, XPS measurement was performed to explore the surface element information of Cu NWs and Cu_2O -on-Cu NWs (Figure 3), in which the numbers of emitted photoelectrons are given as a function of binding energy up to 1000 eV. Three photoemission peaks (Cu 2p, O 1s and C 1s)

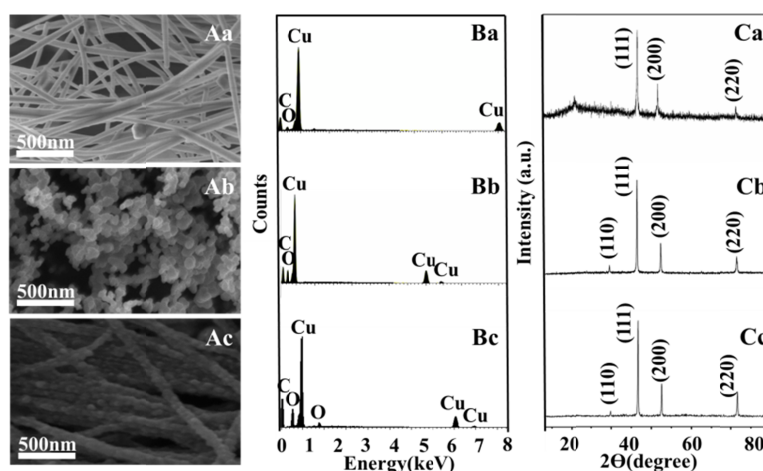


Figure 2. SEM images (Aa-Ac), EDS analysis (Ba-Bc) and XRD patterns (Ca-Cc) of Cu NWs (a), Cu_2O NPs (b) and Cu_2O -on-Cu NWs (c), respectively.

present for wide spectra of Cu₂O-on-Cu NWs and bare Cu NWs in Figure 3A and 3B, respectively. The detailed spectrum of Cu 2p peaks magnified from wide spectrum of Cu₂O-on-Cu NWs in Figure 3C exhibits two peaks at 931.81 eV and 951.86 eV. It's due to the spin-orbit splitting of 2p 3/2 and 2p 1/2, respectively. In order to clarify the exact bonding form of Cu in the Cu₂O-on-Cu NWs, we use XPSPEAK41 to analyse the narrow Cu spectrum. As shown in Figure 3C, the peak of Cu 2p_{2/3} can be split to two peaks as chemical bonding of Cu-Cu bond with different crystal structure and the peak of Cu 2p_{1/2} can be split to two peaks as chemical bonding of pure Cu components (951.2 eV) and Cu-O bond for Cu₂O (952.3 eV). In Figure 3D, the appeared O 1s peak of 530.2 eV further indicates the presence of O species existed as Cu-O bond in Cu₂O. Figure 3E shows the spectrum of bare Cu NWs, as can be observed that there is no shoulder peak exists, indicating that Cu(0) is dominant.

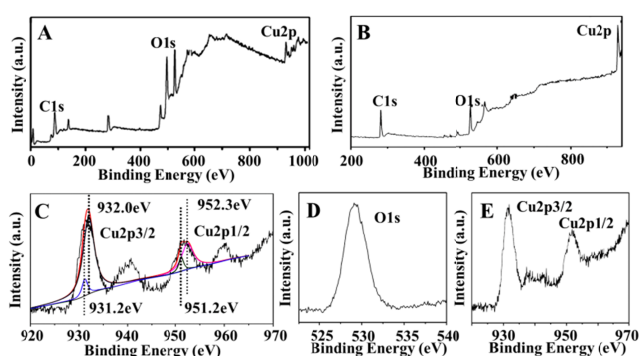
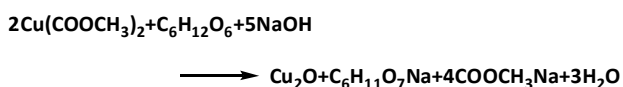


Figure 3. XPS analysis of Cu₂O-on-Cu NWs (A) and Cu NWs (B) with detailed spectra of Cu 2p from Cu₂O in Cu₂O-on-Cu NWs (C) and O 1s (D) as well as Cu 2p from Cu NWs (E).

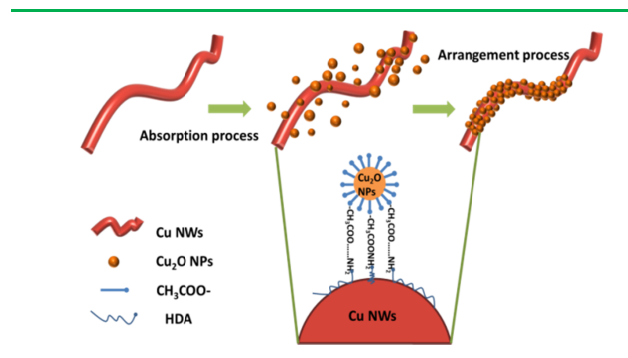
Fabrication Mechanism

Cu₂O-on-Cu heterostructured NWs were synthesized through a facile self-assembly followed in-situ reduction process of Cu²⁺ on Cu NWs surface assisted by structure-director. According to the below equation:



and shown in Scheme 1, after most HDA was rinsed by ethyl alcohol and distilled water, the residual functional HDA molecules were left on the surface of Cu NWs, during the reduction of Cu²⁺ to Cu₂O, the generated -COOCH₃ which were absorbed on the surface of Cu₂O nanoparticles could combined with -NH₂ to -H₂NCOOCH₃-, such self-assembly process results in the attachment of Cu₂O NPs onto the surface of Cu NWs. Apart from this functional group interaction, another contribution comes from hydrophobic interactions between the head groups of the organic capping on the two components. That is, the aliphatic hydrocarbon chains of the two organic components HDA and -COOCH₃ provide them with the noncovalent linkage. Under the two types of binding actions, the obtained composites are very stable considering that they have undergone ultrasonication treatment and several cycles of washing and centrifugation during the

preparation. The products prepared by reaction time from 30 to 90 min and were monitored by SEM images which are shown in Figure S3 in ESI, in which 60 min reaction supplies the best absorption distribution of Cu₂O NPs loaded on Cu NWs.



Scheme 1. Schematic view of the synthesis of Cu₂O-on-Cu NWs.

Photocatalytic Activity

The photocatalytic activity Cu₂O-on-Cu heterostructured NWs was evaluated and compared with other control groups including Cu₂O NPs and Cu NWs toward the photodegradation of RhB, MB and MO under visible-light ($\lambda \geq 420\text{nm}$) irradiation, respectively. Such dye pollutants is presently adopted as a representative organic pollutant in dye wastewater to evaluate the photocatalytic performance of as-prepared photocatalysts at room temperature. The photocatalysis efficiency and the adsorbed amount of RhB, MB and MO were calculated using the concentration of the solution analyzed by UV-filtered visible-light adsorption at a wavelength of 554 nm, 656 nm and 465 nm. The degradation ratio is calculated using the following equations: $y\% = 100 * C/C_0$ (where C_0 and C are the initial and equilibrium concentrations of dye (in mg/L)), which can be described as the absorbance of the solution at the maximized wavelength of 554, 656 and 465 nm (Figure S5 and S6, ESI).

Table 1. Catalytic Activities of bare Cu NWs, Cu₂O NPs and Cu₂O-on-Cu NWs.

catalyst	RhB	MB	MO
Cu NWs	negligible	negligible	negligible
Cu ₂ O NPs	15%	38%	13%
Cu ₂ O-on-Cu NWs	60%	100%	85%

Figure 4 shows the degradation of RhB, MB and MO catalyzed by as-prepared catalysts under visible-light irradiation for evaluating the photocatalytic activities. In order to exclude the possibility of dye pollutants' self-photodegradation, the control experiments of blank samples are proceeding. And it can be observed that the pollutants cannot be degraded no matter how long they are irradiated under visible-light, as shown in Figure S4. In addition, the degradation is negligible to illuminate RhB, MB and MO solution in the presence of bare Cu NWs (Figure 4 and Figure S5). It can be deduced that Cu NWs cannot catalyze the dye

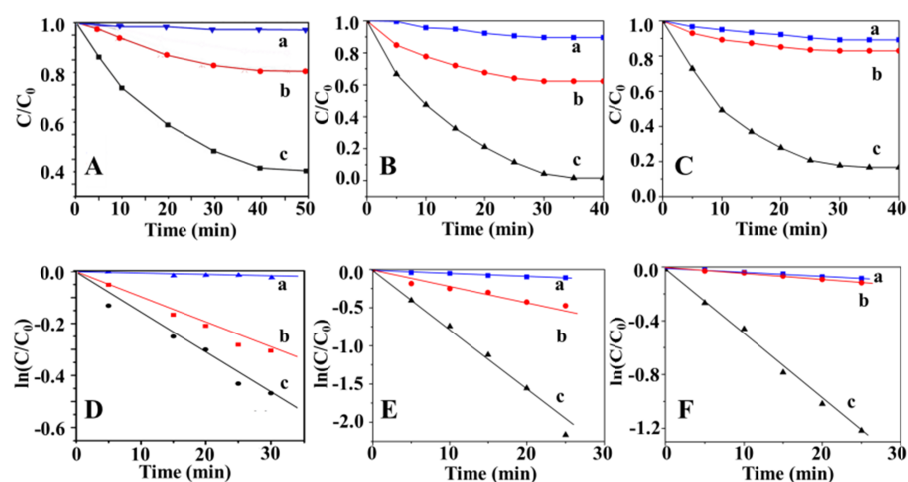


Figure 4. Plots of C/C_0 versus time for the photocatalytic degradation of RhB (A), MB (B) and MO (C) using as-prepared nanocatalysts of Cu NWs (a), Cu_2O NPs (b) and Cu_2O -on-Cu NWs (c) under visible light at r.t. together with their $\ln(C/C_0)$ plots of RhB (D), MB (E) and MO (F). a: Cu NWs; b: Cu_2O NPs; c: Cu_2O -on-Cu NWs.

pollutants directly. The building-blocks of pure phase Cu_2O NPs exhibit similar degradation activity with the degradation rate of about 15%, 38% and 13% for RhB, MB and MO, respectively. As for Cu_2O -on-Cu heterostructured NWs, the photodegradation efficiency toward the degradation of all above three pollutants is much higher than that of pure Cu_2O , and can reach nearly 60%, 100% and 85%. The calculation results are shown in Table 1. This excellent performance can be applied in the visible-light photocatalysis. As plotted in Figure 4D-E, there is a good linear correlation between $\ln(C/C_0)$ and the reaction time (t). It indicates that the photodecomposition reaction of RhB, MB and MO molecules catalyzed by Cu_2O -on-Cu catalysts can be treated as a pseudo-first-order reaction. The rate constants (k) of the photocatalytic degradation of RhB, MB and MO over Cu_2O -on-Cu nanowires are determined to be 0.0137 min^{-1} , 0.0746 min^{-1} and 0.0599 min^{-1} , respectively. Therefore, it is believed that the existence of large interface between the two phases in Cu_2O -on-Cu composites is significant to the excellent visible-light photocatalytic activity. In addition, their UV-vis spectra have been given in Figure S5 and S6 in ESI.

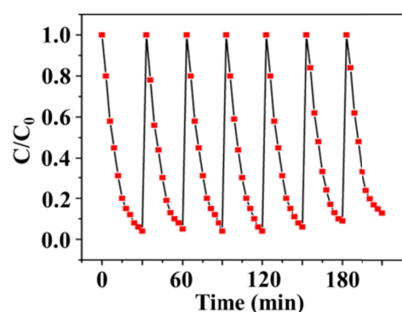
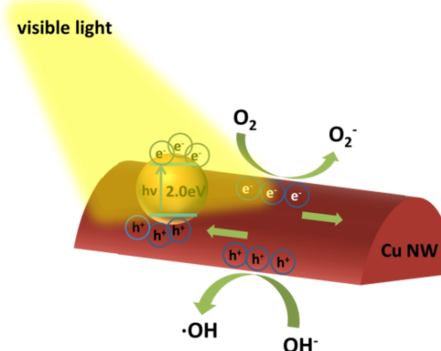


Figure 5. Catalytically recyclable degradation of MB in 7 successive cycles by Cu_2O -on-Cu NWs.

Because the lifetime and stability are important factors for catalyst application, the catalytic activity of Cu_2O -on-Cu nanowires was tested over seven times for the photodegradation of MB under visible-light at room temperature, as shown in Figure 5.

The catalysts can be recycled by centrifugation for at least six successive cycles of reaction without obvious decay in activity. The reaction rate constant was only slightly decreased as compared to fresh catalyst after reusing seven times. And the XRD pattern of Cu_2O -on-Cu nanowires after the degradation of dye pollutant was provided in Figure S8 (ESI) which shows that the phase structure of catalysts didn't change during the catalyzing process. So the as-designed Cu_2O -on-Cu nanowires have excellent stability in the catalytic visible-

light induced photodegradation of MB and are easy to reuse. The morphologies of catalysts before the catalysis and after the seventh catalysis is shown in Figure S7 in ESI. After the photodegradation reaction takes place, the hierarchical structure of the hybrid nanowire is preserved overall with little structural deformation.



Scheme 2. The visible-light-driving photocatalytic mechanism for the degradation of RhB catalyzed by Cu_2O -on-Cu NWs.

To further investigate the photodegradation reaction of dye pollutants such as MB, a proposal mechanism was proposed, and illustrated in Scheme 2. The photocatalysis mechanism of Cu_2O -on-Cu composite for the degradation toward MB can be proposed as the promoted charge separation. As known, three factors can encourage the photocatalytic activity: i) increasing the surface active sites; ii) modifying the band of the semiconductor; iii) hindering the recombination of photogenerated electrons and holes. The band gaps of Cu_2O are 2.0 eV, and the corresponding potentials of its conduction band is -1.4 eV . In our Cu_2O -on-Cu composite system, the interfaces between Cu_2O and Cu effectively increase the electron-hole separation through transferring the photogenerated electrons from the

conduction band of one Cu₂O molecule to that of another Cu₂O molecule through Cu nanowires. Hence, under visible light irradiation, the improvement of the photocatalytic performance is induced by this Cu₂O-on-Cu semiconductor/metal system. The small band gap between the conduction and valence bands allow Cu₂O nanoparticles act as visible light sensitizers in the degradation of MB. As shown in Scheme 2, these photogenerated electrons from Cu₂O molecules are captured and transferred by Cu nanowires; it benefits the charge separation, resulting in a high concentration of holes. Whereas, holes stay in the valence band of Cu₂O to form hole centers. This also hinders the recombination of the photogenerated electrons with the holes. Thus, electrons trapped in Cu nanowires may have a long lifetime and can be transferred to the interface between the composite and solution. In the photocatalytic degradation process of MB, these electrons were transferred to oxygen adsorbed on the surface of Cu to produce a superoxide anion radical ($\cdot\text{O}_2^-$), while the holes can be easily captured by OH⁻ to form a hydroxyl radical species ($\cdot\text{OH}$), which is an extremely strong oxidant for the partial or complete mineralization of organic chemicals.^{4,5,8,33,37} Therefore, the phase interface, acting as electron sinks, promote interfacial charge-transfer kinetics between the metal and semiconductor, improve the separation of photogenerated electron-hole pairs, and then enhance the photocatalytic activity of Cu₂O-on-Cu nanowires photocatalysts. Electrochemical Impedance Spectroscopy (EIS) is an effective tool to study electrolyte effects on electron transport and recombination at the photoanode. It can be obviously observed that Cu₂O-on-Cu NWs have relatively much lower resistance than that of Cu₂O NPs (Figure S9, ESI), it indicates that our strategy could effectively enhance the conductivity and facilitate the oxide reactions at the catalysts/dye pollutants interface. It can be analyzed that the Cu₂O-on-Cu NWs have a good ability of electron transport for the photocatalysis. And it reveals that during the catalysis process, Cu NWs can transport the photoinduced electrons effectively and lower the recombination rate of photoinduced electron/vacancy pairs which further enhance the catalytic performance. The photocatalytic mechanism was partially proved. In addition, the independent extension of nanowire structure makes the active Cu₂O shell of Cu₂O-on-Cu NWs more accessible to MB molecules, resulting in the highest photoactivities.

Conclusions

For developing the visible-light-driving activity of photocatalysts, the Cu₂O-on-Cu heterostructured NWs are constructed through a facile self-assembly followed in-situ reduction approach of Cu₂O NPs on Cu NWs surface assisted by structure-director. The coupling of narrow-band-gap semiconductor Cu₂O NPs and excellent conductor Cu NWs can lead to the markedly enhanced high visible-light photocatalytic activity toward the degradation of dye pollutant including RhB, MO and MB, due to the band-gap adjusting effect and high electron transportation. Additionally, the strong capacity for

oxygen activation of Cu NWs can result in the gathering of negative charges and rich chemisorbed oxygen onto the surface, which can be responsible for high catalytic efficiency of Cu₂O-on-Cu NWs toward the degradation of organic pollutant.

Acknowledgements

This work is financial supported by National Natural Science Foundation (Nos: 21171130, 51271132, 21471114, and 91222103) and 973 Project (No: 2011CB932404) from China.

Notes and references

- 1 J. S. Lee, S. Brittman, D. Yu and H. Park, *J. Am. Chem. Soc.*, 2008, **130**, 6252–6258.
- 2 T. J. Kempa, R. W. Day, S. K. Kim, H. G. Park and C. M. Lieber, *Energy Environ. Sci.*, 2013, **6**, 719–733.
- 3 S. Senapati, S. K. Srivastava, S. B. Singh and H. N. Mishra, *J. Mater. Chem.*, 2012, **22**, 6899–6906.
- 4 H. Y. Hu, Z. B. Jiao, T. Wang, J. H. Ye, G. X. Lu and Y. P. Bi, *J. Mater. Chem. A*, 2013, **1**, 10612–10616.
- 5 Y. P. Bi, H. Y. Hu, S. X. Ouyang, Z. B. Jiao, G. X. Lu and J. H. Ye, *J. Mater. Chem.*, 2012, **22**, 14847–14850.
- 6 G. Filipic and U. Cvelbar, *Nanotechnology*, 2012, **23**, 194001.
- 7 K. R. Krishnadas, P. R. Sajanlal and T. Pradeep, *J. Phys. Chem. C*, 2011, **115**, 4483–4490.
- 8 Y. P. Bi and J. H. Ye, *Chem. Commun.*, 2009, 6551–6553.
- 9 J. Liu, J. Jiang, C. Cheng, H. Li, J. Zhang, H. Gong and H. J. Fan, *Adv. Mater.*, 2011, **23**, 2076–2081.
- 10 A. Paracchino, N. Mathews, T. Hisatomi, M. Stefiik, S. D. Tilley and M. Graetzel, *Energy Environ. Sci.*, 2012, **5**, 8673–8681.
- 11 H. Ko, J. Lee, B. E. Schubert, Y. L. Chueh, P. W. Leu, R. S. Fearing and A. Javey, *Nano Lett.*, 2009, **9**, 2054–2058.
- 12 L. F. Cui, Y. Yang, C. M. Hsu and Y. Cui, *Nano Lett.*, 2009, **9**, 3370–3374.
- 13 C. H. Han, Z. Y. Li, J. Y. Shen, *J. Hazard. Mater.*, 2009, **168**, 215–217.
- 14 H. X. Chen, M. Wen, Z. D. Huang, Q. S. Wu, J. L. Liu and T. Tu, *J. Mater. Chem. A*, 2015, **3**, 600–607.
- 15 a) S. Q. Zhou, M. Wen, N. Wang, Q. S. Wu, Q. N. Wu, and L. Y. Cheng, *J. Mater. Chem.*, 2012, **22** (33), 16858–16864; b) L. Y. Zhou, M. Wen, Q. S. Wu and D. D. Wu, *Dalton Trans.*, 2014, **43**(21), 7924–7929.
- 16 A. Takai, T. Saida, W. Sugimoto, L. Wang, Y. Yamauchi, K. Kuroda, *Chem. Mater.*, 2009, **21**, 3414.
- 17 H. Choi, S. H. Park, *J. Am. Chem. Soc.*, 2004, **126**, 6248.
- 18 Y. Yamauchi, A. Takai, T. Nagaura, S. Inoue, K. Kuroda, *J. Am. Chem. Soc.*, 2008, **130**, 5426.
- 19 C. Guan, X. Xia, N. Meng, Z. Zeng, X. Cao, C. Soci, H. Zhang and H. J. Fan, *Energy Environ. Sci.*, 2012, **5**, 9085–9090.
- 20 L. Yu, G. Zhang, C. Yuan and X. W. Lou, *Chem. Commun.*, 2013, **49**, 137–139.
- 21 D. M. Powell, M. T. Winkler, H. J. Choi, C. B. Simmons, D. B. Needleman and T. Buonassisi, *Energy Environ. Sci.*, 2012, **5**, 5874–5883.
- 22 D. V. Talapin, J. S. Lee, M. V. Kovalenko and E. V. Shevchenko, *Chem. Rev.*, 2010, **110**, 389–458.
- 23 L. B. Hu, D. S. Hecht and G. Gruner, *Chem. Rev.*, 2010, **110**, 5790–5844.
- 24 B. Tian, P. Xie, T. J. Kempa, D. C. Bell and C. M. Lieber, *Nat. Nanotechnol.*, 2009, **4**, 824–829.
- 25 S. K. Kim, R. W. Day, J. F. Cahoon, T. J. Kempa, K. Deok, H. G. Park and C. M. Lieber, *Nano Lett.*, 2012, **12**, 4971–4976.

- 26 L. Cao, J. S. Park, P. Fan, B. Clemens and M. L. Brongersma, *Nano Lett.*, 2010, **10**, 1229–1233.
- 27 J. Tang, Z. Huo, S. Brittman, H. Gao and P. Yang, *Nat. Nanotechnol.*, 2011, **6**, 568–572.
- 28 Y. Yu, V. E. Ferry, A. P. Alivisatos and L. Cao, *Nano Lett.*, 2012, **12**, 3674–3681.
- 29 Z. Liu, Y. Zhan, G. Shi, S. Moldovan, M. Gharbi, L. Song, L. Ma, W. Gao, J. Huang, R. Vajtai, F. Banhart, P. Sharma, J. Lou and P. M. Ajayan, *Nat. Commun.*, 2012, **3**, 879–884.
- 30 X. W. Zou, H. Q. Fan, Y. M. Tian, M. G. Zhang and X. Y. Yan, *Dalton Trans.*, 2015, DOI: 10.1039/c4dt03417a
- 31 E.D. Mishina, K. Nagai, S. Nakabayashi, *Nano Lett.* 2001, **1**, 401.
- 32 S. Chu, X. Zheng, F. Kong, G. Wu, L. Luo, Y. Guo, H. L. Liu, Y. Wang, H. Yu, Z. Zou, *Mater. Chem. Phys.*, 2011, **129**, 1184–1188.
- 33 L. C. Liu, X. R. Gu, C. Z. Sun, H. Li, Y. Deng, F. Gao, L. Dong, *Nanoscale*, 2012, **4**, 6351–6359.
- 34 L. Xiong, F. Yang, L. Yan, N. Yan, X. Yang, M. Qiu, Y. Yu, *J. Phy. Chem. Sol.* 2011, **72**, 1104–1109.
- 35 S. Z. Oener, S. A. Mann, B. Sciacca, C. Sfiligoj, J. Hoang and E. C. Garnett, *Appl. Phys. Lett.* 2015, 106.
- 36 K. M. Pan, H. Ming, H. Yu, H. Huang, Y. Liu and Z. H. Kang, *Dalton Trans.*, 2012, **41**, 2654.
- 37 J. L. Liu, M. Wen, H. X. Chen, J. Li and Q. S. Wu, *ChemPlusChem*, 2014, **79**, 298–303.